iScience

CellPress
OPEN ACCESS

Article

Insight into an Oxidative DNA-Cleaving DNAzyme: Multiple Cofactors, the Catalytic Core Map and a Highly Efficient Variant

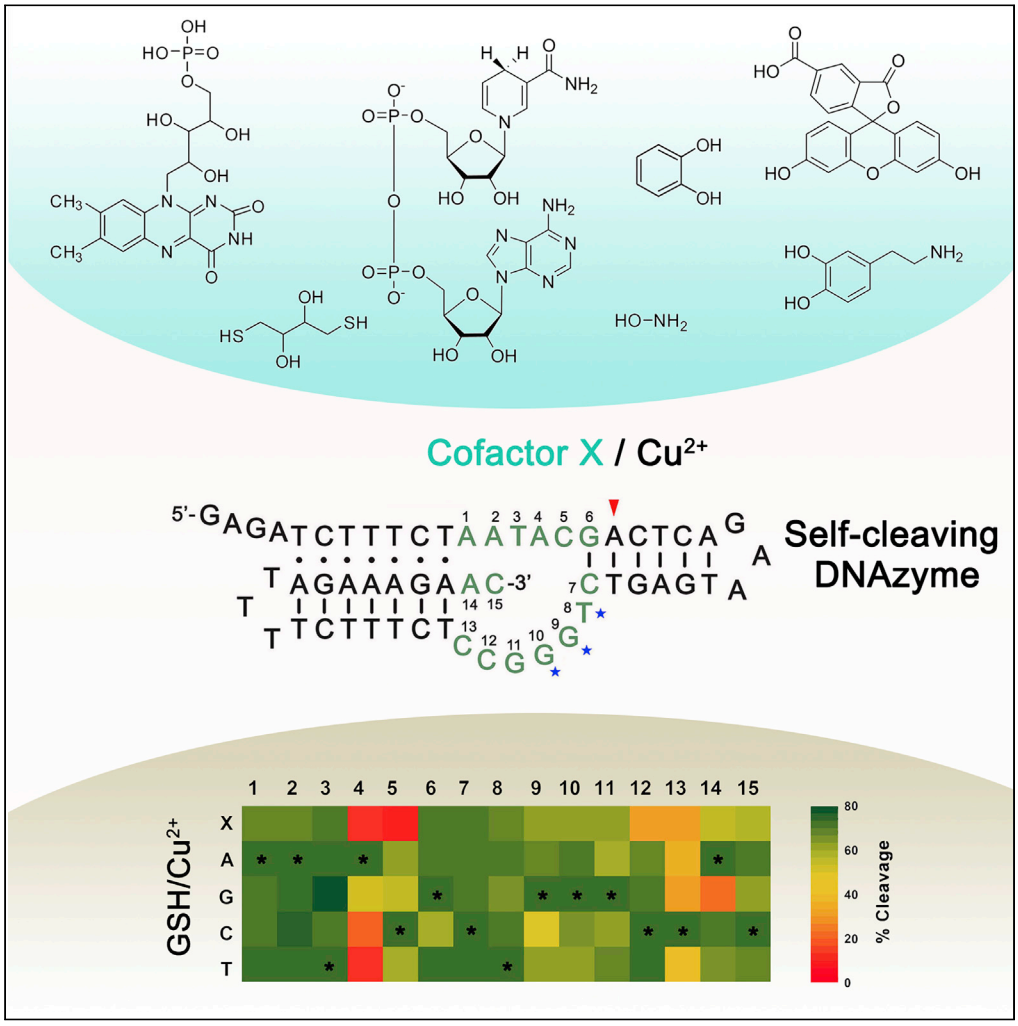

Wenqian Yu, Shijin Wang, Dongling Cao, ..., Jin Zhang, Jiacui Xu, Dazhi Jiang

jcxu@jlu.edu.cn (J.X.)
jiangdz@jlu.edu.cn (D.J.)

HIGHLIGHTS

An oxidative cleavage DNAzyme works with various cofactor X

Catalytic nucleotide conservation fluctuates with different cofactor X

The PL DNAzyme's minor secondary structure change affects electrophoretic mobility

Double-cofactor model of the variant T3G can be converted to sole-cofactor model

Yu et al., iScience *23*, 101555
October 23, 2020
https://doi.org/10.1016/j.isci.2020.101555

iScience

CellPress
OPEN ACCESS

Article

Insight into an Oxidative DNA-Cleaving DNAzyme: Multiple Cofactors, the Catalytic Core Map and a Highly Efficient Variant

Wenqian Yu,[1,4] Shijin Wang,[1,3,4] Dongling Cao,[1] Hongyue Rui,[1] Chengcheng Liu,[1] Yongjie Sheng,[1] Yanhong Sun,[1] Jin Zhang,[1] Jiacui Xu,[2,*] and Dazhi Jiang[1,5,*]

SUMMARY

An oxidative DNA-cleaving DNAzyme (PL) employs a double-cofactor model "X/Cu^{2+}" for catalysis. Herein, we verified that reduced nicotinamide adenine dinucleotide (NADH), flavin mononucleotide, cysteine, dithiothreitol, catechol, resorcinol, hydroquinone, phloroglucinol, *o*-phenylenediamine, 3,3′,5,5′-tetramethylbenzidine, and hydroxylamine acted as cofactor X. According to their structural similarities or fluorescence property, we further confirmed that reduced nicotinamide adenine dinucleotide phosphate (NADPH), 2-mercaptoethanol, dopamine, chlorogenic acid, resveratrol, and 5-carboxyfluorescein also functioned as cofactor X. Superoxide anions might be the commonality behind these cofactors. We subsequently determined the conservative change of individual nucleotides in the catalytic core under four different cofactor X. The nucleotides A4 and C5 are highly conserved, whereas the conservative levels of other nucleotides are dependent on the types of cofactor X. Moreover, we observed that the minor change in the PL's secondary structure affects electrophoretic mobility. Finally, we characterized a highly efficient variant T3G and converted its double-cofactor NADH/Cu^{2+} to sole-cofactor NADH.

INTRODUCTION

DNAzymes, also called deoxyribozymes, are DNA oligonucleotides that have the capability of performing catalytic functions. Breaker and Joyce reported the first DNAzyme that catalyzed the Pb^{2+}-dependent cleavage of an RNA phosphoester in 1994 (Breaker and Joyce, 1994). Since then, a variety of DNAzymes have been isolated by *in vitro* selection and most catalyze site-specific cleavage of nucleic acid substrates (Hollenstein, 2015; Liu et al., 2017; Silverman, 2015, 2016). As DNA only contains four different nitrogenous bases, to exert DNA's catalytic potential, metal ions are typically required for DNAzyme catalysis (McGhee et al., 2017; Zhou and Liu, 2018; Zhou et al., 2017). For example, the 10–23 DNAzyme works with Mg^{2+}, Ca^{2+}, Mn^{2+}, Pb^{2+}, etc. (Chen et al., 2004); the Tm7 DNAzyme can use three lanthanide ions including Ho^{3+}, Er^{3+}, and Tm^{3+}(Huang et al., 2015); and the 10MD5 DNAzyme needs Zn^{2+} and Mn^{2+} to facilitate cleavage (Chandra et al., 2009). Some DNAzymes even have stringent requirements for metal ions, such as NaA43 works only with Na^{+} (Torabi et al., 2015), Ag10c is strictly dependent on Ag^{+} (Saran and Liu, 2016), I-R3 enables the use of Zn^{2+} as the sole cofactor for catalysis (Gu et al., 2013), and 39E is UO_2^{2+} dependent (Liu et al., 2007). According to the relationships between cofactors and DNAzymes, various DNAzyme-based biosensors have been developed. Liu group designed a series of DNAzyme biosensors for lanthanide ions detection in water and integrated them into a test matrix (Huang et al., 2016). Lu group applied the NaA43, 8–17, and 39E DNAzymes for imaging of Na^{+}, Zn^{2+}, and UO_2^{2+} in living cells, respectively (Hwang et al., 2014; Wang et al., 2017b; Wu et al., 2013, 2017). Li and co-workers developed a biosensor to detect *Clostridium difficile* using the RFD-CD1 DNAzyme (Shen et al., 2016) and further constructed the RFD-EC1 and DHp3T4 DNAzymes into paper sensors for sensing *E. coli* and *Helicobacter pylori*, respectively (Ali et al., 2011, 2017, 2019).

In 1996, Breaker group reported oxidative DNA-cleaving DNAzymes isolated by *in vitro* selection. Most individual DNAzymes that were selected after eight rounds of selection conformed to two distinct classes (Carmi et al., 1996). After that, beginning with the original seventh round DNA population, they carried

[1]Key Lab for Molecular Enzymology & Engineering of the Ministry of Education, School of Life Sciences, Jilin University, 2699# Qianjin Street, Changchun 130012, China

[2]College of Animal Sciences, Jilin University, 5333# Xi'an Road, Changchun 130062, China

[3]Present address: Zhangdian No.8 Middle School, 298# Huaguang Road, Zhangdian District, Zibo 255020, China

[4]These authors contributed equally

[5]Lead Contact

*Correspondence: jcxu@jlu.edu.cn (J.X.), jiangdz@jlu.edu.cn (D.J.)

https://doi.org/10.1016/j.isci.2020.101555

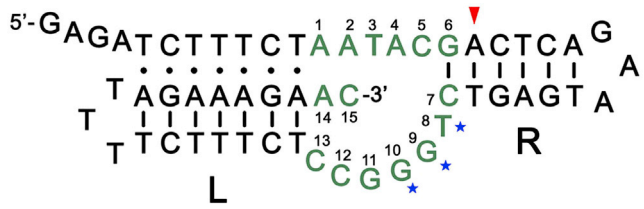

Figure 1. The Sequence and Secondary Structure of the PL DNAzyme

The green letters correspond to the nucleotides within the catalytic core. The red arrowhead and the blue asterisks, respectively, indicate the major and minor sites of DNA cleavage. L and R designate stem-loop structures, where lines indicate Watson-Crick base pairs and dots represent triple helix interactions.

out an additional six rounds of *in vitro* selection. Finally, they obtained a highly active "class II" DNAzyme (PL) with a pistol-like secondary structure through sequence optimization (Carmi et al., 1998; Carmi and Breaker, 2001). PL employed a double-cofactor model "X/Cu^{2+}" for catalysis. Its activity was low in the presence of Cu^{2+} alone and greatly increased with the addition of cofactor X, such as vitamin C (VC) or hydrogen peroxide (H_2O_2). As PL was taken as a Cu^{2+}-dependent DNAzyme, it has been applied to develop many Cu^{2+} biosensors (Chen et al., 2016a, 2016b; Fang et al., 2010; Li et al., 2013; Liu and Lu, 2007; Yin et al., 2009; Wang et al., 2010b, Wang et al., 2017a, 2017b; Wu et al., 2010; Tian et al., 2016). Our previous study showed that vitamin B_2 (VB_2), pyrogallol (PG), and reduced glutathione (GSH) can also function as cofactor X (Sun et al., 2017; Wang et al., 2017a). Based on these clues, we scanned 30 different chemical compounds and verified that some of them can act as cofactor X. Moreover, on the basis of their chemical structures and characters, we speculated that some of their derivatives could perform a similar function. The experimental results are in line with our expectation. Analysis of the commonality behind these diversified cofactor X will directly help to determine the boundary of cofactor X, and also to deeply understand the catalytic mechanism of PL.

A DNAzyme normally contains a catalytic core responsible for catalysis. The nucleotides within the catalytic core were originally obtained through *in vitro* selection, followed by site mutation assays to determine whether the nucleotides are conserved or not. These non-conserved nucleotides can become suitable modification sites. Modified nucleotides are likely to improve the functional properties of these DNAzymes (Hollenstein, 2019; Wang et al., 2018a, 2018b), which would provide the basis for further studies on the catalytic mechanisms for DNAzymes. The catalytic cores of the 8–17 and 10–23 DNAzymes have been well studied by modified nucleotides (Li et al., 2014; Räz and Hollenstein, 2015; Wang et al., 2010a). Lu et al. employed modified nitrogen bases (guanine analogs) to analyze the reaction mechanism of the 8–17 DNAzyme and proved that it is a general acid-base catalysis (Cepeda-Plaza et al., 2018). However, the relationship studies about the activities and the nucleotides within the catalytic cores under different types of cofactors are very less. We speculate that conservation of these nucleotides will change with different cofactors. In this article, we mapped the relationships between PL mutations and their catalytic activities under four groups of cofactors (three of them are newly found). Results demonstrated that the nucleotides conservation was affected by the types of cofactors. Meanwhile, the determined non-conserved nucleotides would provide the targets for rational design of this DNAzyme. In addition, we found that single-nucleotide mutation resulted in the DNA migration change in the electrophoresis, indicating that DNA migration is not totally determined by the molecular weight of DNA, also influenced by the minor change in DNA structure. Through mutation, we obtained an efficient variant and characterized its activity changes under different conditions. The variant itself, the optimized reaction condition and these newly found sulfydryl-containing cofactors can be further applied to improve our designed Cu^{2+} biosensor (Wang et al., 2017a).

RESULTS AND DISCUSSION

Multiple Cofactors of PL

The PL construct used in this study is shown in Figure 1. PL self-cleaves at multiple sites, generally requiring VC/Cu^{2+} or H_2O_2/Cu^{2+} for catalysis (Carmi et al., 1996, 1998; Carmi and Breaker, 2001; Jiang et al., 2010). Our recent study showed that VB_2/Cu^{2+}, GSH/Cu^{2+}, and PG/Cu^{2+} also enabled to yield the cleavage products (Sun et al., 2017; Wang et al., 2017a). Based on these known cofactors, we tested the effects of 30 different compounds (four types: vitamins, sulfydryls, phenolics, and amines) on PL catalysis (Figure 2A).

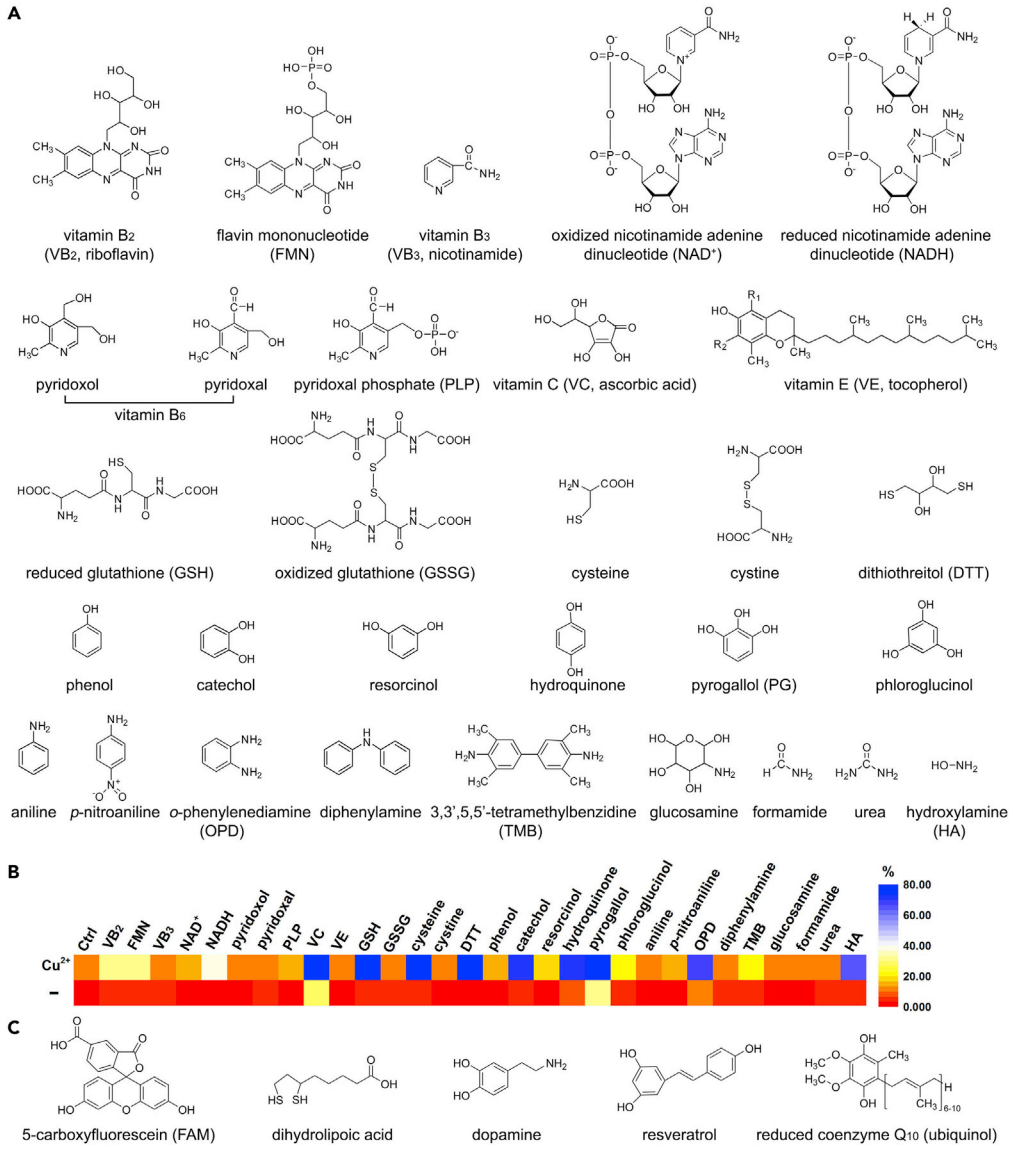

Figure 2. Chemical Structures of Small Compounds and Their Effects on PL Catalysis

(A) Thirty types of chemical compounds and their structures.

(B) Effects of 30 types of chemical compounds on PL. PL (0.5 μM) was incubated with 100 μM compound at 23°C for 1 h in a mixture containing 100 μM Cu^{2+} (or none), 300 mM NaCl, and 50 mM Tris-HCl (7.0). The reaction system containing VB_2 or FMN needs to be performed in white light.

(C) Chemical structures of some cofactor X of PL.

Among vitamins (Figure 2A), VC (ascorbic acid) is the most common cofactor X of PL. According to its antioxidant property, we further chose vitamin E (VE, tocopherol) and three forms of vitamin B_6 including pyridoxol, pyridoxal, and also pyridoxal phosphate (PLP) for tests. Experimental results reconfirmed the oxidative role of VC in PL catalysis, although to our knowledge VC is a widely used antioxidant. However, unlike VC, VE and vitamin B_6 failed to support PL cleavage either with or without Cu^{2+}, implying that antioxidant property was not a reliable basis for screening cofactor X of PL (Figure 2B). Meanwhile, taking into account the fact that oxidation of reduced nicotinamide adenine dinucleotide (NADH) occurs simultaneously with the formation of superoxide anions in the electron respiratory chain (Hirst, 2013; Vinogradov and Grivennikova, 2016), we speculated that NADH could enable PL cleavage, whereas oxidized nicotinamide adenine dinucleotide (NAD^+) could not. Therefore, we evaluated the effects of NADH, NAD^+, and also vitamin B_3 (VB_3, nicotinamide) on PL. As expected, in the presence of Cu^{2+}, NADH supported substantial catalysis, whereas neither NAD^+ nor nicotinamide did. Apparently, reduced

nicotinamide adenine dinucleotide phosphate (NADPH) (Figure 2C), the analog of NADH, is probably a new cofactor X of PL, which has been verified by the experimental results (Figure S1). Although NADH alone was not sufficient for PL catalysis (Figure 2B), an efficient PL variant could only use NADH to support the oxidative-cleavage reaction, which was confirmed in the following study (see the section "Characterization of T3G"). In addition, based on the effect of VB_2 (riboflavin) on PL, we investigated the function of its analog flavin mononucleotide (FMN). Intriguingly, the fluorophore molecule FMN initiated a light-dependent self-cleavage of PL (Figure 2B), possibly due to the formation of reactive oxygen species such as superoxide anion by light excitation of the fluorescent molecules (Icha et al., 2017; Kim et al., 2015). This has been applied to 5-carboxyfluorescein (FAM) (Figures 2C and S1). Thus, PL can become a light-regulated catalyst in the presence of fluorophores, wherein its catalytic activity is related to the intensity and wavelength of light.

For sulfydryl compounds (Figure 2A), the effect of reduced glutathione (GSH) on PL has been confirmed in our previous study (Wang et al., 2017a), in which GSH alone did not enable PL cleavage, but combination with Cu^{2+} supported substantial catalysis. Besides, oxidized glutathione (GSSG) did not work with PL. Thus, sulfydryl group in GSH is the key for PL catalysis. According to this, we chose cysteine and dithiothreitol (DTT) for examination; meanwhile GSSG and cystine were taken as the negative controls. As shown in Figure 2B, GSH, cysteine, DTT rather than GSSG, and cystine aided PL cleavage in the presence of Cu^{2+}, and all sulfydryl compounds failed to support PL catalysis in the absence of Cu^{2+}, consistent with our expectation. Moreover, the analog of DTT, 2-mercaptoethanol, was also a cofactor X and supported self-cleavage of PL (Figures 2C and S1). In addition, dihydrolipoic acid and coenzyme A are both sulfydryl-containing compounds and could play a similar role (Figure S2).

The effect of PG (benzene-1,2,3-triol) on PL activity has been determined in our previous report (Sun et al., 2017). Therefore, taking into account the chemical structure of PG, we did a systematic study using phenolic compounds, differing in the number and position of the hydroxyl groups on the benzene rings. The six tested compounds were PG (benzene-1,2,3-triol), phloroglucinol (benzene-1,3,5-triol), catechol (benzene-1.2-diol), resorcinol (benzene-1,3-diol), hydroquinone (benzene-1,4-diol), and phenol (Figure 2A). As shown in Figure 2B, in the presence of Cu^{2+}, all phenolic compounds except phenol were able to support PL function, and the high catalytic activities were observed when treated with catechol, hydroquinone, PG, and phloroglucinol, respectively. In the absence of Cu^{2+}, PL had a higher activity with PG and had weak activities with catechol, hydroquinone, or phloroglucinol. As similar chemical structures normally relate to similar functions, we speculated that dopamine, chlorogenic acid (analogs of catechol), and resveratrol (analog of resorcinol) could also act as cofactor X (Figure 2C), which have been confirmed as shown in Figure S1. Based on the aforementioned results, we thought that the analogs of dopamine, levodopa, norepinephrine, and epinephrine are probably cofactor X. Even the reduced coenzyme Q_{10} (the analog of hydroquinone) and gallic acid monohydrate (the analog of PG) could support PL catalysis (Figure S2).

Among amine compounds, *o*-phenylenediamine (OPD) leads to DNA damage in the presence of Cu^{2+} (Bolt and Golka, 2007; Murata et al., 2006). Therefore, according to the structure of OPD, we further selected aniline, *p*-nitroaniline, diphenylamine, and 3,3′,5,5′-tetramethylbenzidine (TMB) for PL assays, in which aniline was taken as a negative control (Figure 2A). Hydroxylamine (HA) was also chosen for tests, because it can modify unpaired cytosine to induce DNA cleavage, chemical cleavage of mismatch (Tabone et al., 2006). The chemical structure of HA is very simple, consisting of ammonia bearing a hydroxyl substituent (Figure 2A). Similar to HA, formamide had an aldehyde group instead of a hydroxyl group. Besides, urea substitutes a hydrogen bonded to a carbon atom with an amino group, compared with formamide. Moreover, glucosamine was also reported to cleave DNA in the presence of Cu^{2+} (Watanabe et al., 1990). Thus, the aforementioned compounds were chosen for examination. Data showed that when Cu^{2+} was present, PL had significant catalytic activities with OPD or HA, whereas trace activity with TMB. In the absence of Cu^{2+}, only OPD supported cleavage product formation (Figure 2B). In addition, according to the effects and chemical structure of OPD, its analogs *p*-phenylenediamine and *m*-phenylenediamine may also have the similar function (Figure S2).

Analysis of Oxidative DNA Cleavage

Collectively, the aforementioned results revealed that many compounds with various chemical structures can act as cofactor X for PL catalysis. What is the commonality behind these cofactor X? In general, hydroxyl radicals are thought to be the main reason for DNA damage; however, our study excluded its possibility to participate in PL catalysis (Sun et al., 2017). Although hydrogen peroxide is closely related to PL catalysis, it

is not a direct factor (Sun et al., 2017). Superoxide anion is able to unify these cofactor X, which might directly attack a carbon in nucleoside for strand scission, similarly as observed in RadDz3 DNAzyme (Lee et al., 2017). Oxidation of some cofactor X is accompanied by electron transfer. The dissolved oxygen can take electrons to form superoxide anion. For example, catechol reacts with oxygen to generate *o*-quinone and superoxide anion (Equation 1). Superoxide anion can be further turned into hydrogen peroxide (Equation 2) (Sawyer et al., 1985) that directly reacts with Cu^{2+} for superoxide anion formation (Equation 3) (Pham et al., 2013). This explains why catechol alone can result in PL cleavage and the addition of Cu^{2+} greatly increases its cleavage yield (Figure 2B). This catalytic mechanism model works with VC, PG, OPD, and NADH, but is not suitable for sulfydryl-containing cofactor X, which alone cannot help PL for catalysis and only works when it combines with Cu^{2+}. Thus, another catalytic mechanism model is necessary to explain how sulfydryl-containing cofactor X functions in PL catalysis. We take DTT as an example, which itself is a reductant for protein reduction and cannot react with oxygen to generate superoxide anion. However, DTT can reduce Cu^{2+} into Cu^{+} (Equation 4), which further reacts with oxygen to form Cu^{2+} and superoxide anion (Equation 5) (Kachur et al., 1997). Therefore, DTT must combine with Cu^{2+} to function (Figure 2B). Based on these analyses, we believe that the boundary of the cofactors of PL lies in the compounds that can produce superoxide anions. From another perspective, PL as a DNA is a safe and highly efficient superoxide anion scavenge, suitable for inhibiting cell damage caused by superoxide anion.

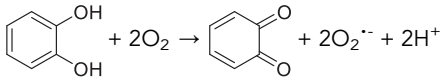

$$+ 2O_2 \rightarrow + 2O_2^{\bullet -} + 2H^+ \qquad \text{(Equation 1)}$$

$$2O_2^{\bullet -} + 2H^+ \rightarrow H_2O_2 + O_2 \qquad \text{(Equation 2)}$$

$$Cu^{2+} + H_2O_2 \rightarrow Cu^{+} + 2H^+ + O_2^{\bullet -} \qquad \text{(Equation 3)}$$

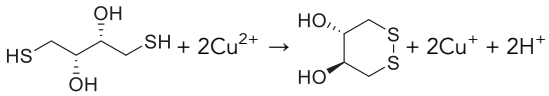

$$+ 2Cu^{2+} \rightarrow + 2Cu^{+} + 2H^+ \qquad \text{(Equation 4)}$$

$$Cu^{+} + O_2 \rightarrow Cu^{2+} + O_2^{\bullet -} \qquad \text{(Equation 5)}$$

Mapping the Catalytic Core of PL

We have identified various chemical compounds able to support PL catalysis. In this section, we further determine the relationship between the nucleotides within the catalytic core of PL and its cofactors, to confirm the essential nucleotides for PL catalysis and to analyze the conservation tendency of nucleotides under various cofactors.

In the context of PL shown in Figure 1, 11 deletions and 15 single-site substitutions were introduced at the core positions to carry out a comprehensive mutational study of PL motif. Totally 56 variants were investigated under four kinds of representative cofactors including VC/Cu^{2+}, GSH/Cu^{2+}, PG/Cu^{2+}, and HA/Cu^{2+} (Figure 3A and Table S1). These cofactors are chosen on the basis of the following reasons. VC is the most commonly used cofactor for the PL DNAzyme. GSH is a very efficient cofactor and performs important roles in cells. PG and HA are the best cofactors of phenolic and amine compounds, respectively.

In the presence of VC/Cu^{2+}, analysis results from 11 deletion variants showed that A4 and C5 were strictly conserved and that each deletion was substantially impaired in catalysis, with about 6-fold drop in cleavage yield. Besides, any deletion at the positions C12, C13, A14, and C15 led to about 2-fold decrease in activity. However, deletion of any other nucleotide (A1-T3, G6-G11) only caused a small decrease in catalysis. A similar deletion mutation pattern was also observed in the presence of GSH/Cu^{2+} or HA/Cu^{2+} (Figure 3A). However, when PG/Cu^{2+} were present, all deletion variants lost their activities dramatically, exhibiting a high degree of conservation of these nucleotides (Figure 3A).

In the presence of VC/Cu^{2+}, single-site substitutional analysis revealed that substitutions at each of A1, A2, T3, C7, C12, and C15 positions seemed relatively well tolerated, the best yield observed from the T3G variant. In addition, C5 and C13 were conserved, as any substitution led to decreased activity. Moreover, substitutions of A4 and G9 with purine reduced the cleavage yield about 20% and with pyrimidine

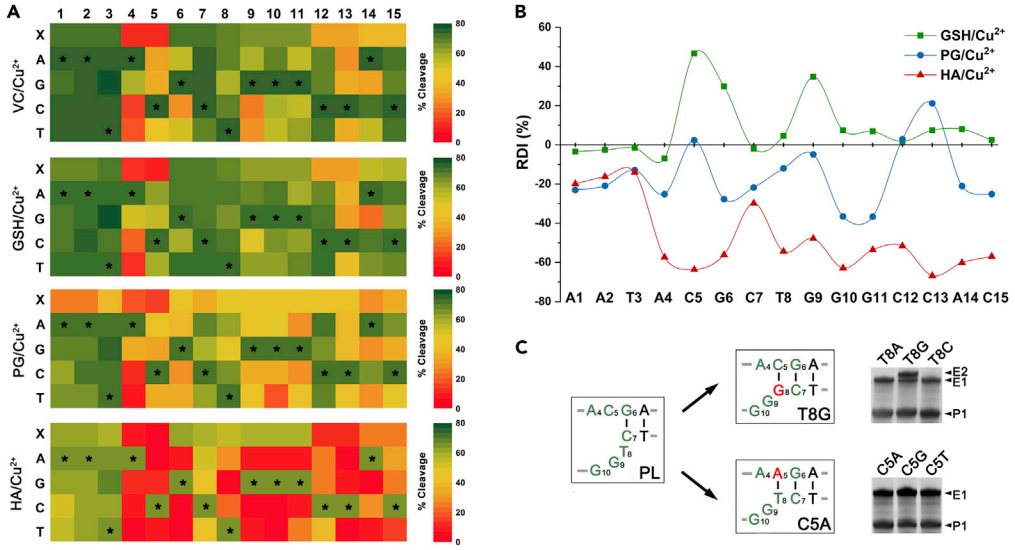

Figure 3. Analysis of Single-Site Variants within the Catalytic Core of PL

(A) Heatmaps summarizing the cleavage yield (%) for single-site variants under four groups of cofactors. Colored blocks with asterisks indicate the original PL nucleotides.

(B) Relative drift intensity (RDI) of the nucleotides within the core of PL.

(C) Single-site mutation affects electrophoretic mobility.

produced 5- and 3-fold drop in catalysis. Replacement of A14 with guanine impaired catalysis, with about 2.5-fold drop in cleavage yield, and replacement with cytosine retained activity comparable to that of the parent canonical construct. Substitution of G10 and G11 led to similar effects; any substitution only retained partial activity. Substitutions of C12 and C15 caused only small changes in catalysis.

The impact patterns of PL's substitutional variants under four kinds of cofactors were compared and summarized in the following (Figure S3): A1, A2, and T3 were highly tolerant nucleotides, beneficial to restore or increase PL activity, which are ideal modification sites for rational design of PL, such as chemical modification. The T3G variant always had a higher activity than PL when treated with any kind of cofactors; A4 was conservative, and any substitution mutation resulted in a severe functional defect; C5 was highly tolerant to substitution mutation with GSH/Cu^{2+}, but was relatively conserved with other cofactors. Substitution mutations from G6 to C12 caused small changes in catalysis in the presence of GSH/Cu^{2+} and led to significant changes when treated with HA/Cu^{2+}; C13 was the most strictly conserved nucleotide with any kind of cofactors. The substitutions of A14 with guanine seriously negatively affected the catalytic activity, and substitution with pyrimidine retained the most activity in the presence of VC/Cu^{2+} or GSH/Cu^{2+}. An opposite result was observed when substitution mutations of A14 were treated with HA/Cu^{2+} or PG/Cu^{2+}; C15 was relatively variable with VC/Cu^{2+} or GSH/Cu^{2+}, but its conservation increased when treated with HA/Cu^{2+} or PG/Cu^{2+}.

PL is a multiple cofactors-dependent DNAzyme. As shown in Figure S3, the impacts of PL variants differently changed depending on the type of cofactors. We applied "relative drift intensity (RDI)" to describe the fluctuation in nucleotide conservation and took the overall activities of single-nucleotide mutations with VC/Cu^{2+} as the baseline (Figure 3B). In general, the degree of nucleotide conservation in PL decreased with GSH/Cu^{2+} and major decreases were observed at C5, G6, and G9; the degree of nucleotide conservation majorly improved with PG/Cu^{2+}, and only C13 exhibited a reduced conservation. In addition, all nucleotides showed increased conservation when treated with HA/Cu^{2+}, especially C5, G10, and C13.

For gel-based PL catalytic assay, we observed a small mobility difference in the T8G mutant on the electrophoresis gel among 56 variants. A slower migrating band E2 appeared above the band E1 where PL variants were positioned (Figure 3C). In terms of molecular weight, mutation of thymidine at position 8 to guanine only increases 25 Dalton, which is not sufficient to change the electrophoretic mobility compared with the molecular weight of PL (17,277 Dalton). According to the single-strand conformation polymorphism,

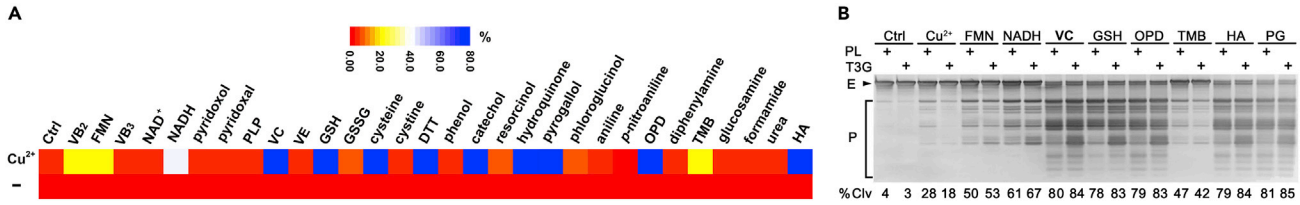

Figure 4. T3G Catalysis in the Presence of Different Cofactors

(A) The effects of 30 types of chemical compounds on T3G.

(B) Comparison of T3G and PL by treatment with eight kinds of cofactors. T3G and PL were incubated with 100 μM cofactor at 23°C for 1 h in a mixture containing 100 μM Cu^{2+}, 300 mM NaCl, and 50 mM Tris-HCl (pH 7.0). E and P represent the PL DNAzyme and cleavage fragments, respectively.

single-site mutation in single-stranded DNA sequence allows the sequence to be distinguished by gel electrophoresis, which separates fragments based on their different conformations (Orita et al., 1989). In T8G, formation of a base pair between guanine at position 8 and cytidine at position 5 induced a conformational change and resulted in a slower migration on gel electrophoresis. However, in C5A mutant, adenine at position 5 and thymidine at position 8 also can form a stable base pair to change its secondary structure, but its DNA mobility was unchanged. This is likely due to the poor stability of AT base pair compared with CG base pair. In 7 M urea denaturing gel, part of the CG base pair in T8G opened, forming a normal mobility E1 band; the rest of CG base pair was retained, generating a slower mobility E2 band. In contrast, all AT base pairs in C5A were disrupted under denaturing conditions and only produced E1 band. Therefore, conformational effect of CG base pair is stronger than AT base pair, indicating that single-nucleotide change is sufficient to affect DNA migration in electrophoresis.

Characterization of T3G

Among all PL variants, T3G is highly efficient with each of VC/Cu^{2+}, GSH/Cu^{2+}, PG/Cu^{2+}, and HA/Cu^{2+}. Thus, we further evaluated the activity change of T3G with more compounds (Figure 4A). In the presence of Cu^{2+}, T3G worked better with VB_2, FMN, NADH, VC, GSH, cysteine, DTT, catechol, hydroquinone, PG, OPD, TMB, and HA. However, T3G had no observable activity in the absence of Cu^{2+}, which allows us to improve our early developed biosensor for Cu^{2+} detection with much lower test background (Wang et al., 2017a). Based on Figure 4A, we subsequently measured and compared the cleavage yields of T3G and PL, using Cu^{2+} with each of FMN, NADH, VC, GSH, OPD, TMB, HA, and PG (Figure 4B). When Cu^{2+} or TMB/Cu^{2+} was present, PL was more active than T3G, but in both cases there was low yield; cleavage reactions of T3G and PL with FMN/Cu^{2+} or NADH/Cu^{2+} were much effective than using TMB/Cu^{2+} or Cu^{2+} alone; when treated with VC/Cu^{2+}, GSH/Cu^{2+}, OPD/Cu^{2+}, HA/Cu^{2+}, or PG/Cu^{2+}, T3G performed a stronger self-cleavage activity than PL. In addition, PL exhibited weak activities when treated with VC or OPD alone, but T3G had no observable activity in this case (Figure S4).

According to the aforementioned results and considering the biological significance of NADH and GSH, we chose NADH/Cu^{2+} and GSH/Cu^{2+} as cofactors to characterize enzymatic properties of T3G. We first investigated the effect of pH on T3G catalysis (Figure 5A). Results showed that the asymmetrical-shaped V curves were observed both in NADH/Cu^{2+} and GSH/Cu^{2+}. In both cases, T3G had high and steady activities in the range of pH 5.0 to 7.0, with decreased activities from pH 7.0 to 8.4. Surprisingly, the activity of T3G gradually increased from pH 8.4 to 9.0, possibly due to non-specific DNA cleavage caused by alkaline conditions. Overall, slight acidic condition is beneficial for T3G activity. A similar pH curve was observed with the PL DNAzyme in our previous report (Wang et al., 2017a), indicating that PL mutation at position T3 did not change the pH dependence of PL. We further characterized the effects of NaCl and KCl on T3G activity (Figure 5B). Data showed that NaCl and KCl were both favorable to increase T3G activity. When cofactor was NADH/Cu^{2+}, NaCl and KCl performed similarly, T3G activity increased with the increase of NaCl or KCl. When cofactor was GSH/Cu^{2+}, NaCl and KCl slightly impacted T3G activity, reaching a plateau over 200 mM, with a slightly higher yield observed in NaCl. Unlike T3G, NaCl can significantly increase the PL activity (Wang et al., 2017a), indicating that mutation of T3G reduced sensitivity to NaCl concentration. In the following, we detected the effect of incubation temperature on T3G (Figure 5C). In the presence of NADH/Cu^{2+}, T3G activity increased with the increase of temperature, with the maximum yield observed at 40°C. In the presence of GSH/Cu^{2+}, T3G activity was slightly changed, reaching a plateau over 23°C. Data showed that T3G was slightly affected by the incubation temperature and can still maintain a

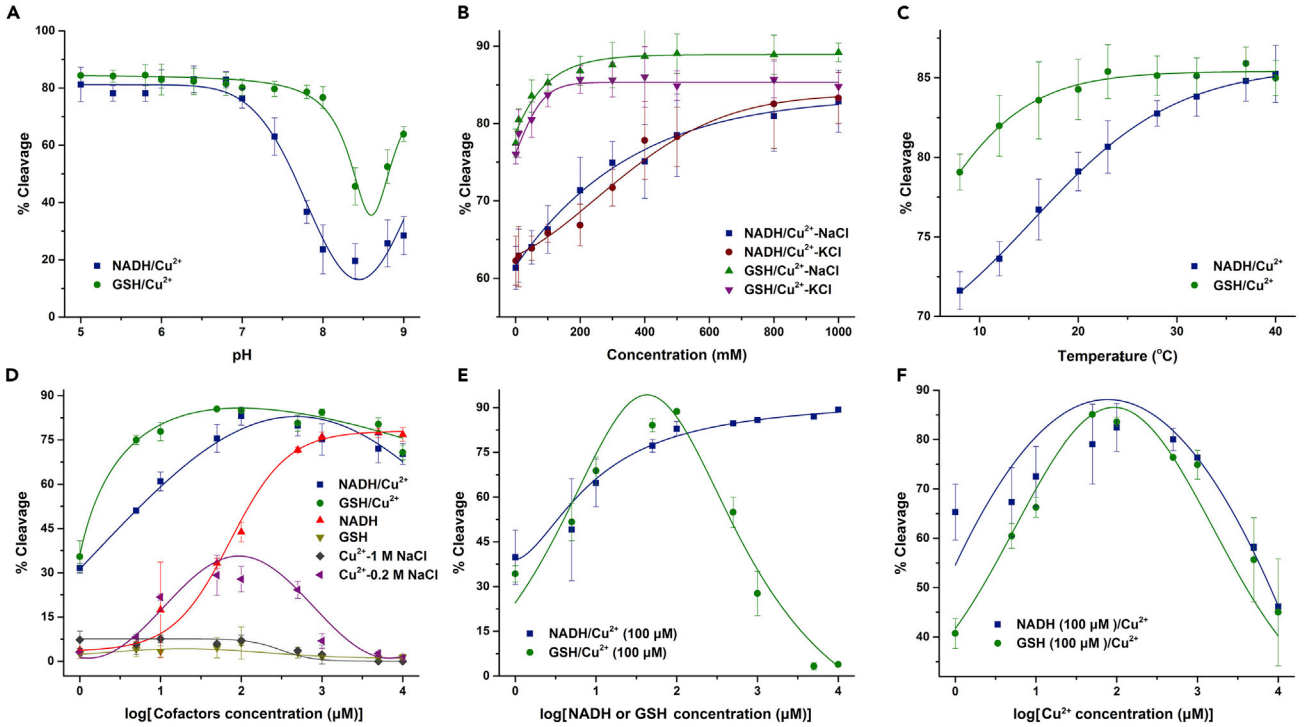

Figure 5. Enzymatic Characterization of T3G

(A) pH-dependent activity of T3G in the presence of NADH/Cu^{2+} and GSH/Cu^{2+}. Reactions were conducted at 50 mM pH buffer (pH 5.0–9.0).

(B) The effects of NaCl and KCl on T3G function. Reactions were conducted with 1–1,000 mM NaCl (KCl).

(C) The effect of temperature on T3G activity. Reactions were conducted with 1 M NaCl within 8–40°C.

(D) The effects of components (NADH/Cu^{2+}, GSH/Cu^{2+}, NADH, GSH, Cu^{2+}-1M NaCl, Cu^{2+}-0.2 M NaCl) of reaction solution on T3G activity. Refer to "Transparent Methods" for the specific composition and concentration of cofactors used in Figure 5D.

(E) The effects of NADH and GSH on T3G activity in the presence of 100 μM Gu^{2+}. (F) The effects of Cu^{2+} on T3G activity in the presence of either 100 μM NADH or 100 μM GSH. The error bars represented the standard deviations from three repeated measurements.

high activity with GSH/Cu^{2+} at low temperature, implying that oxidative DNA cleavage catalyzed by DNAzymes is not sensitive to the reaction temperature in the presence of GSH/Cu^{2+}. This property would help us improve the construction of PL-based Cu^{2+} biosensors (Wang et al., 2017a). In addition, the impacts of different concentrations of various cofactors on T3G were measured (Figures 5D–5F). As shown in Figure 5D, in the presence of NADH/Cu^{2+} or GSH/Cu^{2+}, T3G activity first increased and then decreased, the best yields obtained at 500 μM NADH/Cu^{2+} and 50 μM GSH/Cu^{2+}, respectively. Under optimized conditions, T3G activity significantly increased in the range from 10 to 1,000 μM NADH, indicating that NADH alone is sufficient to support T3G catalysis. This can be explained by the fact that NADH can form superoxide anion with oxygen (Equation 6) (Vinogradov and Grivennikova, 2016), and further supported the superoxide anion-induced catalytic mechanism of PL.

$$NADH + 2O_2 \rightarrow NAD^+ + 2O_2^- + H^+ \qquad \text{(Equation 6)}$$

When GSH was present, T3G had no observable activity, consistent with our previous study. In the presence of Cu^{2+} and 1 M NaCl, T3G showed a very weak activity, but in the presence of 200 mM NaCl, T3G activity first increased and then decreased with the increase of Cu^{2+}, showing a bell-shaped curve and obtaining the best yield at 100 μM. Furthermore, the effects of NADH and GSH on T3G activity were evaluated in the presence of 100 μM Cu^{2+} (Figure 5E). T3G cleavage yield gradually increased with the increase of NADH, but first increased and then decreased with the increase of GSH, with the best yield at 100 μM. Finally, the effect of Cu^{2+} on T3G was tested, when the concentration of NADH or GSH was 100 μM. Similar curve was observed in both cases, in which T3G activity first increased and then decreased.

Based on the results shown in Figure 5, we confirmed the effects of Cu^{2+} on T3G. Cu^{2+} alone only resulted in a slight T3G cleavage, but can enhance the effect of NADH on T3G and is necessary for the function of GSH

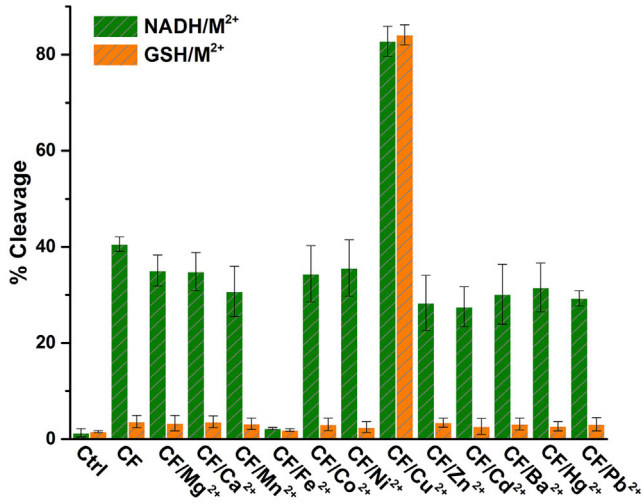

Figure 6. The Effects of Divalent Metal Ions on T3G Activity

T3G was incubated with 100 μM NADH (or GSH) and 100 μM metal ions at 23°C for 1 h in a mixture containing 1 (or 0.2) M NaCl and 50 mM MES (pH 6.4). Fe^{2+} led to DNA aggregation in gel wells and affected DNA migration. CF indicates NADH and GSH. The error bars represented the standard deviations from three repeated measurements.

on T3G. As shown in Figure 6, we further tested the effects of Mg^{2+}, Ca^{2+}, Mn^{2+}, Fe^{2+}, Co^{2+}, Ni^{2+}, Zn^{2+}, Cd^{2+}, Ba^{2+}, Hg^{2+}, and Pb^{2+} on T3G. Data indicated that these metal ions did not improve T3G activity in the presence of NADH or GSH. In addition, we compared the cleavage rate of T3G and PL in the presence of NADH (Figure S5), with a k_{obs} of 0.021 and 0.037 min^{-1}, respectively. The fact that the activity of T3G was lower than that of PL in the presence of NADH seems inconsistent with the fact that T3G is the best variant. Actually T3G is the most efficient variant in the presence of cofactor X/Cu^{2+}," indicating that Cu^{2+} is more effective in enhancing T3G catalysis. To verify this idea, we compared the cleavage rates of T3G and PL in the presence of NADH/Cu^{2+} and GSH/Cu^{2+} (Figures S6 and S7). T3G and PL exhibited k_{obs} values of 0.119 min^{-1} and 0.103 min^{-1} in the presence of NADH/Cu^{2+} and 0.172 min^{-1} and 0.151 min^{-1} in the presence of GSH/Cu^{2+}, respectively. In the reaction system, addition of Cu^{2+} can speed up the reactions of T3G and PL, attaining 50% yield at 9.6 min and 17.8 min with NADH/Cu^{2+} and 4.7 min and 7.3 min with GSH/Cu^{2+}, but at 84.2 min and 53.6 min with NADH alone (no activity was observed for both T3G and PL in the presence of GSH alone).

In our previous study, we have used the PL DNAzyme to develop a Cu^{2+} biosensor (Wang et al., 2017a). T3G is a highly active mutant, whose catalytic activity is greatly affected by the concentration of Cu^{2+}. This property can improve our designed PL-based Cu^{2+} biosensor to mainly increase its detection sensitivity. T3G is not sensitive to VC, OPD, or PG and can further reduce the detection background. Furthermore, the catalytic activity of T3G is less affected by the reaction temperature, which can enhance the stability of the Cu^{2+} biosensor to adapt to different environment temperatures. In addition, using isothermal DNA amplification and rolling circle amplification as the signal amplification element for construction of T3G-based Cu^{2+} biosensor it is possible to achieve ultra-sensitive detection of Cu^{2+}.

Conclusion

In this study, we first scanned the chemical compounds suitable for PL catalysis and found its various cofactor X with different chemical structures, such as NADH, FMN, cysteine, DTT, catechol, OPD, TMB, and HA. According to these newly obtained cofactors, we further suspected and verified that some of their derivatives such as NADPH, FAM, 2-mercaptoethanol, dopamine, chlorogenic acid, and resveratrol were also cofactor X of PL. Through analysis of these cofactor X, we proposed that the catalytic mechanism of PL might be superoxide anion-mediated DNA oxidative cleavage, which would help to define the boundary of PL cofactors. This proposed catalytic mechanism is also likely to be applicable to other oxidative DNA-cleaving DNAzymes, which might "share" these newly discovered cofactors. Subsequently, mutational analysis of PL within its catalytic core indicated that the nucleotide conservation changed with different cofactors, which might also apply to other multi-cofactor-dependent DNAzymes. Moreover,

the identified non-conservative nucleotides can be used as the artificial modification targets to add new features for DNAzymes. For example, modification of a DNAzyme with a photocaged group, 2′-O-nitrobenzyl adenosine, maybe used to develop a UV light-regulated DNAzyme (Wu et al., 2017). In addition, we found that the minor change in the secondary structure of the variant T8G can affect its electrophoretic mobility. This phenomenon is not unique to PL mutants, and has been observed in the I-R3 DNAzyme's mutants (Cao et al., 2020). Finally, we characterized an efficient variant T3G. The fact that T3G activity can depend upon sole cofactor NADH further supported our proposed catalytic mechanism of PL. This variant can be applied to improve our designed PL-based biosensors (Wang et al., 2017a) and maybe also applicable for *in vivo* RNA imaging and DNA logic gates (Wei et al., 2020; Banno et al., 2019).

Limitations of the Study

Although we have found a variety of cofactors for the PL DNAzyme and speculated that PL catalyzed cleavage is related to superoxide anions according to its various cofactors, we have not yet obtained the data showing the formation of superoxide anions in the reaction system. During the study of PL variants, we only obtained a highly active mutant and further performed many characterizations of this mutant, but we have not yet fully understood why this mutant has an improved catalytic activity. It is mainly because PL's three-dimensional structure has not been reported. In future, a combination of cofactors, mutants, and structure of PL could provide a new way to deeply explore its catalytic mechanism.

Resource Availability

Lead Contact

Further information and requests for resources and reagents should be directed to and will be fulfilled by the Lead Contact, Dazhi Jiang (jiangdz@jlu.edu.cn).

Materials Availability

This study did not generate new unique reagents.

Data and Code Availability

This study did not generate/analyze datasets/code.

METHODS

All methods can be found in the accompanying Transparent Methods supplemental file.

SUPPLEMENTAL INFORMATION

Supplemental Information can be found online at https://doi.org/10.1016/j.isci.2020.101555.

ACKNOWLEDGMENTS

We thank Dr. Lei Wang, Dr. Zhi Wang, and Dr. Ming Lv for valuable discussions. This study was supported by the National Natural Science Foundation of China (31700747), Science and Technology Development Program of Jilin Province (20180101251JC), and Science Research Program of Jilin Province during the 13th Five-Year Plan Period (JJKH20170817KJ).

AUTHOR CONTRIBUTIONS

D.J. and J.X. designed the experiments. D.J., W.Y., S.W., D.C., H.R. and C.L. performed the experiments. D.J., J.X., Y. Sheng, Y. Sun, and J.Z. analyzed data. J.X. and D.J. wrote the manuscript.

DECLARATION OF INTERESTS

The authors declare no competing interests.

Received: April 15, 2020
Revised: August 24, 2020
Accepted: September 9, 2020
Published: October 23, 2020

REFERENCES

Ali, M.M., Aguirre, S.D., Lazim, H., and Li, Y. (2011). Fluorogenic DNAzyme probes as bacterial indicators. Angew. Chem. Int. Ed. *50*, 3751–3754.

Ali, M.M., Brown, C.L., Jahanshahi-Anbuhi, S., Kannan, B., Li, Y., Filipe, C.D.M., and Brennan, J.D. (2017). A printed multicomponent paper sensor for bacterial detection. Sci. Rep. *7*, 12335.

Ali, M.M., Wolfe, M., Tram, K., Gu, J., Filipe, C.D.M., Li, Y., and Brennan, J.D. (2019). A DNAzyme-based colorimetric paper sensor for helicobacter pylori. Angew. Chem. Int. Ed. *58*, 9907–9911.

Banno, A., Higashi, S., Shibata, A., and Ikeda, M. (2019). A stimuli-responsive DNAzyme displaying boolean logic-gate responses. Chem. Commun. *55*, 1959–1962.

Bolt, H.M., and Golka, K. (2007). The debate on carcinogenicity of permanent hair dyes: new insights. Crit. Rev. Toxicol. *37*, 521–536.

Breaker, R.R., and Joyce, G.F. (1994). A DNA enzyme that cleaves RNA. Chem. Biol. *1*, 223–229.

Cao, D., Yu, W., Wang, F., Jiang, Y., Sheng, Y., Sun, Y., Zhang, J., Xu, J., and Jiang, D. (2020). Characterization of a DNA-hydrolyzing DNAzyme for generation of PCR strands of unequal length. Biochimie In press.

Carmi, N., Balkhi, S.R., and Breaker, R.R. (1998). Cleaving DNA with DNA. Proc. Natl. Acad. Sci. U S A *95*, 2233–2237.

Carmi, N., and Breaker, R.R. (2001). Characterization of a DNA-cleaving deoxyribozyme. Bioorg. Med. Chem. *9*, 2589–2600.

Carmi, N., Shultz, L.A., and Breaker, R.R. (1996). *In vitro* selection of self-cleaving DNAs. Chem. Biol. *3*, 1039–1046.

Cepeda-Plaza, M., McGhee, C.E., and Lu, Y. (2018). Evidence of a general acid-base catalysis mechanism in the 8-17 DNAzyme. Biochemistry *57*, 1517–1522.

Chandra, M., Sachdeva, A., and Silverman, S.K. (2009). DNA-catalyzed sequence-specific hydrolysis of DNA. Nat. Chem. Biol. *5*, 718–720.

Chen, F., Wang, R., Li, Z., Liu, B., Wang, X., Sun, Y., Hao, D., and Zhang, J. (2004). A novel replicating circular DNAzyme. Nucleic Acids Res. *32*, 2336–2341.

Chen, Y., Chen, L., Ou, Y., Wang, Z., Fu, F., and Guo, L. (2016a). DNAzyme-based biosensor for Cu^{2+} ion by combining hybridization chain reaction with fluorescence resonance energy transfer technique. Talanta *155*, 245–249.

Chen, Y., Zhou, D., Meng, Z., and Zhai, J. (2016b). An ion-gating multinanochannel system based on a copper-responsive self-cleaving DNAzyme. Chem. Commun. *52*, 10020–10023.

Fang, Z., Huang, J., Lie, P., Xiao, Z., Ouyang, C., Wu, Q., Wu, Y., Liu, G., and Zeng, L. (2010). Lateral flow nucleic acid biosensor for $Cu2^{+}$ detection in aqueous solution with high sensitivity and selectivity. Chem. Commun. *46*, 9043–9045.

Gu, H., Furukawa, K., Weinberg, Z., Berenson, D.F., and Breaker, R.R. (2013). Small, highly active DNAs that hydrolyze DNA. J. Am. Chem. Soc. *135*, 9121–9129.

Hirst, J. (2013). Mitochondrial complex I. Annu. Rev. Biochem. *82*, 551–575.

Hollenstein, M. (2015). DNA catalysis: the chemical repertoire of DNAzymes. Molecules *20*, 20777–207804.

Hollenstein, M. (2019). Nucleic acid enzymes based on functionalized nucleosides. Curr. Opin. Chem. Biol. *52*, 93–101.

Huang, P.J., Vazin, M., Lin, J., Pautler, R., and Liu, J. (2016). Distinction of individual lanthanide ions with a DNAzyme beacon array. ACS Sens. *1*, 732–738.

Huang, P.J., Vazin, M., Matuszek, Ż., and Liu, J. (2015). A new heavy lanthanide-dependent DNAzyme displaying strong metal cooperativity and unrescuable phosphorothioate effect. Nucleic Acids Res. *43*, 461–469.

Hwang, K., Wu, P., Kim, T., Lei, L., Tian, S., Wang, Y., and Lu, Y. (2014). Photocaged DNAzymes as a general method for sensing metal ions in living cells. Angew. Chem. Int. Ed. *53*, 13798–13802.

Icha, J., Weber, M., Waters, J.C., and Norden, C. (2017). Phototoxicity in live fluorescence microscopy, and how to avoid it. Bioessays *39*, 1700003.

Jiang, D., Xu, J., Sheng, Y., Sun, Y., and Zhang, J. (2010). An allosteric DNAzyme with dual RNA-cleaving and DNA-cleaving activities. FEBS J. *277*, 2543–2549.

Kachur, A.V., Held, K.D., Koch, C.J., and Biaglow, J.E. (1997). Mechanism of production of hydroxyl radicals in the copper-catalyzed oxidation of dithiothreitol. Radiat. Res. *147*, 409–415.

Kim, K., Park, H., and Lim, K.M. (2015). Phototoxicity: its mechanism and animal alternative test methods. Toxicol. Res. *31*, 97–104.

Lee, Y., Klauser, P.C., Brandsen, B.M., Zhou, C., Li, X., and Silverman, S.K. (2017). DNA-catalyzed DNA cleavage by a radical pathway with well-defined products. J. Am. Chem. Soc. *139*, 255–261.

Li, H., Huang, X., Kong, D., Shen, H., and Liu, Y. (2013). Ultrasensitive, high temperature and ionic strength variation-tolerant Cu^{2+} fluorescent sensor based on reconstructed Cu^{2+}-dependent DNAzyme/substrate complex. Biosens. Bioelectron. *42*, 225–228.

Li, Z., Liu, Y., Liu, G., Zhu, J., Zheng, Z., Zhou, Y., and He, J. (2014). Position-specific modification with imidazolyl group on 10-23 DNAzyme realized catalytic activity enhancement. Bioorg. Med. Chem. *22*, 4010–4017.

Liu, J., Brown, A.K., Meng, X., Cropek, D.M., Istok, J.D., Watson, D.B., and Lu, Y. (2007). A catalytic beacon sensor for uranium with parts-per-trillion sensitivity and millionfold selectivity. Proc. Natl. Acad. Sci. U S A *104*, 2056–2061.

Liu, J., and Lu, Y. (2007). A DNAzyme catalytic beacon sensor for paramagnetic Cu^{2+} ions in aqueous solution with high sensitivity and selectivity. J. Am. Chem. Soc. *129*, 9838–9839.

Liu, M., Chang, D., and Li, Y. (2017). Discovery and biosensing applications of diverse RNA-cleaving DNAzymes. Acc. Chem. Res. *50*, 2273–2283.

McGhee, C.E., Loh, K.Y., and Lu, Y. (2017). DNAzyme sensors for detection of metal ions in the environment and imaging them in living cells. Curr. Opin. Biotechnol. *45*, 191–201.

Murata, M., Nishimura, T., Chen, F., and Kawanishi, S. (2006). Oxidative DNA damage induced by hair dye components ortho-phenylenediamines and the enhancement by superoxide dismutase. Mutat. Res. *607*, 184–191.

Orita, M., Iwahana, H., Kanazawa, H., Hayashi, K., and Sekiya, T. (1989). Detection of polymorphisms of human DNA by gel electrophoresis as single-strand conformation polymorphisms. Proc. Natl. Acad. Sci. U S A *86*, 2766–2770.

Pham, A.N., Xing, G., Miller, C.J., and Waite, T.D. (2013). Fenton-like copper redox chemistry revisited: hydrogen peroxide and superoxide mediation of copper-catalyzed oxidant production. J. Catal. *301*, 54–64.

Räz, M.H., and Hollenstein, M. (2015). Probing the effect of minor groove interactions on the catalytic efficiency of DNAzymes 8-17 and 10-23. Mol. Biosyst. *11*, 1454–1461.

Saran, R., and Liu, J. (2016). A silver DNAzyme. Anal. Chem. *88*, 4014–4020.

Sawyer, D.T., Calderwood, T.S., Johlman, C.L., and Wilkins, C.L. (1985). Oxidation by superoxide ion of catechols, ascorbic acid, dihydrophenazine, and reduced flavins to their respective anion radicals. A common mechanism via a combined proton-hydrogen atom transfer. J. Org. Chem. *50*, 1409–1412.

Shen, Z., Wu, Z., Chang, D., Zhang, W., Tram, K., Lee, C., Kim, P., Salena, B.J., and Li, Y. (2016). A catalytic DNA activated by a specific strain of bacterial pathogen. Angew. Chem. Int. Ed. *55*, 2431–2434.

Silverman, S.K. (2015). Pursuing DNA catalysts for protein modification. Acc. Chem. Res. *48*, 1369–1379.

Silverman, S.K. (2016). Catalytic DNA: scope, applications, and biochemistry of deoxyribozymes. Trends Biochem. Sci. *41*, 595–609.

Sun, Y., Ma, R., Wang, S., Li, G., Sheng, Y., Rui, H., Zhang, J., Xu, J., and Jiang, D. (2017). New cofactors and inhibitors for a DNA-cleaving DNAzyme: superoxide anion and hydrogen peroxide mediated an oxidative cleavage process. Sci. Rep. *7*, 378.

Tabone, T., Sallmann, G., Chiotis, M., Law, M., and Cotton, R. (2006). Chemical cleavage of mismatch (CCM) to locate base mismatches in heteroduplex DNA. Nat. Protoc. *1*, 2297–2304.

Tian, R., Chen, X., Liu, D., and Yao, C. (2016). A sensitive biosensor for determination of Cu^{2+} by one-step electrodeposition. Electroanalysis *28*, 1617–1624.

Torabi, S.F., Wu, P., McGhee, C.E., Chen, L., Hwang, K., Zheng, N., Cheng, J., and Lu, Y. (2015). *In vitro* selection of a sodium-specific DNAzyme and its application in intracellular sensing. Proc. Natl. Acad. Sci. U S A *112*, 5903–5908.

Vinogradov, A.D., and Grivennikova, V.G. (2016). Oxidation of NADH and ROS production by respiratory complex I. Biochim. Biophys. Acta *1857*, 863–871.

Wang, B., Cao, L., Chiuman, W., Li, Y., and Xi, Z. (2010a). Probing the function of nucleotides in the catalytic cores of the 8-17 and 10-23 DNAzymes by abasic nucleotide and C3 spacer substitutions. Biochemistry *49*, 7553–7562.

Wang, S., Liu, C., Li, G., Sheng, Y., Sun, Y., Rui, H., Zhang, J., Xu, J., and Jiang, D. (2017a). The triple roles of glutathione for a DNA-cleaving DNAzyme and development of a fluorescent glutathione/Cu^{2+}-dependent DNAzyme sensor for detection of Cu^{2+} in drinking water. ACS Sens. *2*, 364–370.

Wang, W., Satyavolu, N.S.R., Wu, Z., Zhang, J., Zhu, J., and Lu, Y. (2017b). Near-infrared photothermally activated DNAzyme-gold nanoshells for imaging metal ions in living cells. Angew. Chem. Int. Ed. *56*, 6798–6802.

Wang, Y., Liu, E., Lam, C.H., and Perrin, D.M. (2018a). A densely modified M^{2+}-independent DNAzyme that cleaves RNA efficiently with multiple catalytic turnover. Chem. Sci. *9*, 1813–1821.

Wang, Y., Ngor, A.K., Nikoomanzar, A., and Chaput, J.C. (2018b). Evolution of a general RNA-cleaving FANA enzyme. Nat. Commun. *9*, 5067.

Wang, Y., Yang, F., and Yang, X. (2010b). Label-free colorimetric biosensing of copper(II) ions with unimolecular self-cleaving deoxyribozymes and unmodified gold nanoparticle probes. Nanotechnology *21*, 205502.

Watanabe, K., Kashige, N., Kojima, M., and Nakashima, Y. (1990). Specificity of nucleotide sequence in DNA cleavage induced by D-glucosamine and D-glucosamine-6-phosphate in the presence of Cu^{2+}. Agric. Biol. Chem. *54*, 519–525.

Wei, J., Wang, H., Wu, Q., Gong, X., Ma, K., Liu, X., and Wang, F. (2020). A smart, autocatalytic, DNAzyme biocircuit for *in vivo*, amplified, microRNA imaging. Angew. Chem. Int. Ed. *59*, 5965–5971.

Wu, C.S., Khaing Oo, M.K., and Fan, X. (2010). Highly sensitive multiplexed heavy metal detection using quantum-dot-labeled DNAzymes. ACS Nano *4*, 5897–5904.

Wu, P., Hwang, K., Lan, T., and Lu, Y. (2013). A DNAzyme-gold nanoparticle probe for uranyl ion in living cells. J. Am. Chem. Soc. *135*, 5254–5257.

Wu, Z., Fan, H., Satyavolu, N.S.R., Wang, W., Lake, R., Jiang, J., and Lu, Y. (2017). Imaging endogenous metal ions in living cells using a DNAzyme-catalytic hairpin assembly probe. Angew. Chem. Int. Ed. *56*, 8721–8725.

Yin, B., Ye, B., Tan, W., Wang, H., and Xie, C. (2009). An allosteric dual-DNAzyme unimolecular probe for colorimetric detection of copper(II). J. Am. Chem. Soc. *131*, 14624–14625.

Zhou, W., and Liu, J. (2018). Multi-metal-dependent nucleic acid enzymes. Metallomics *10*, 30–48.

Zhou, W., Saran, R., and Liu, J. (2017). Metal sensing by DNA. Chem. Rev. *117*, 8272–8325.

iScience, Volume *23*

Supplemental Information

Insight into an Oxidative DNA-Cleaving DNAzyme: Multiple Cofactors, the Catalytic Core Map and a Highly Efficient Variant

Wenqian Yu, Shijin Wang, Dongling Cao, Hongyue Rui, Chengcheng Liu, Yongjie Sheng, Yanhong Sun, Jin Zhang, Jiacui Xu, and Dazhi Jiang

Supplemental Information

Insight into an oxidative DNA-cleaving DNAzyme: multiple cofactors, the catalytic core map and a highly efficient variant

Wenqian Yu, Shijin Wang, Dongling Cao, Hongyue Rui, Chengcheng Liu, Yongjie Sheng, Yanhong Sun, Jin Zhang, Jiacui Xu, and Dazhi Jiang

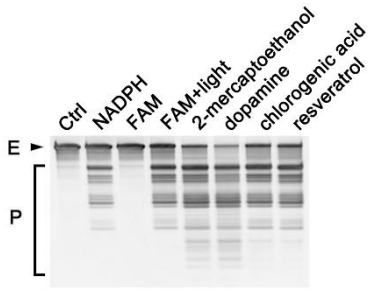

Figure S1, related to Figure 2. Effects of cofactor X on PL.

PL (0.5 μM) was incubated with 100 μM cofactor X at 23 °C for 1 hr in a mixture containing 100 μM Cu^{2+}, 300 mM NaCl and 50 mM Tris-HCl (7.0). The reaction system containing FAM needs to performed in dark environment or under a sunlight lamp. E and P represent the PL DNAzyme and cleavage fragments, respectively.

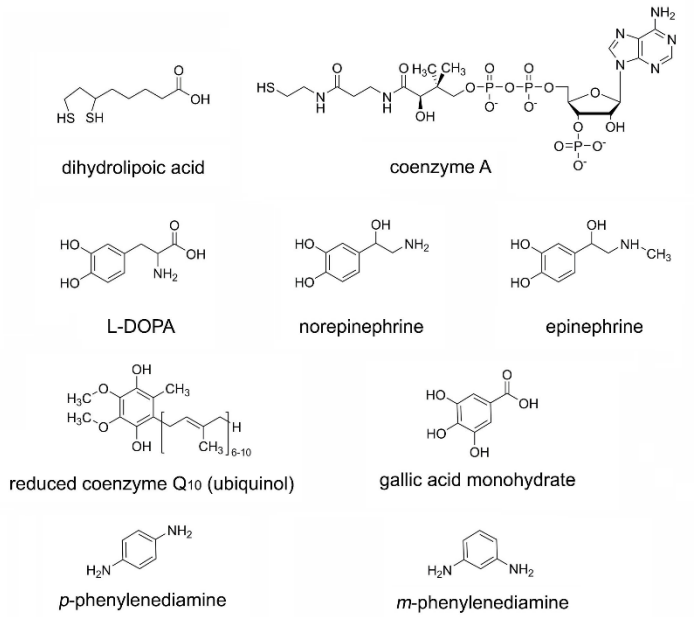

Figure S2, related to Figure 2. Structures of chemical compounds that are presumed to be cofactor X of the PL DNAzyme.

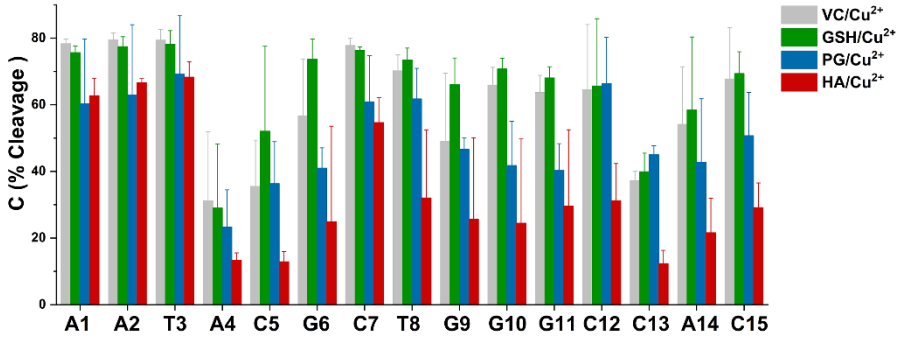

Figure S3, related to Figure 3. Tendencies in catalytic activities of single-point variants within catalytic core of PL under various cofactors.

C=(C_{N1}+C_{N2}+C_{N3}+C_{N4})/4, C indicates the average cleavage yield of single nucleotide variants at N position.

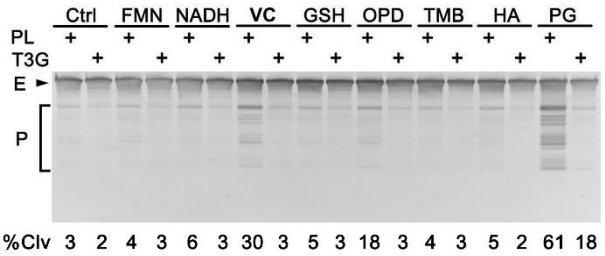

Figure S4, related to Figure 4. Comparison of T3G and PL by treatment with 8 kinds of cofactors without Cu^{2+}.

T3G and PL were incubated with 100 μM cofactor at 23 °C for 1 hr in a mixture containing 300 mM NaCl and 50 mM Tris-HCl (pH 7.0). E represents the PL and T3G DNAzymes, and P represents cleavage fragments.

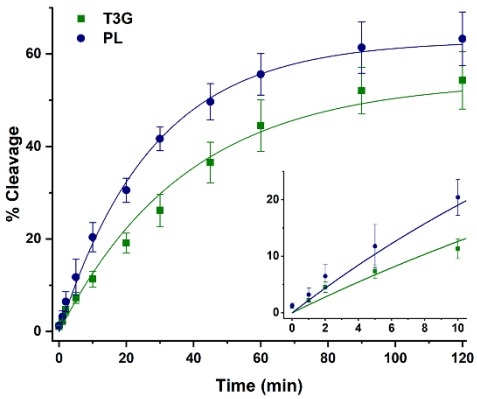

Figure S5, related to Figure 5. Cleavage yields of T3G and PL over the time in the presence of NADH. 0.5 μM T3G (or PL) was incubated with 100 μM NADH at 23 °C in a mixture containing 1 M NaCl and 50 mM MES (pH 6.4). The error bars represented the standard deviations from three repeated measurements.

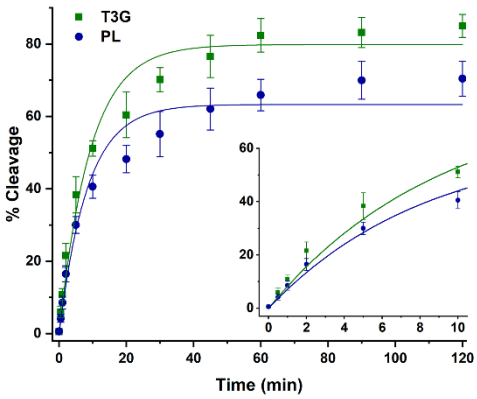

Figure S6, related to Figure 5. Cleavage yields of T3G and PL over the time in the presence of NADH/Cu^{2+}. 0.5 μM T3G (or PL) was incubated with 100 μM NADH/Cu^{2+} at 23 °C in a mixture containing 1 M NaCl and 50 mM MES (pH 6.4). The error bars represented the standard deviations from three repeated measurements.

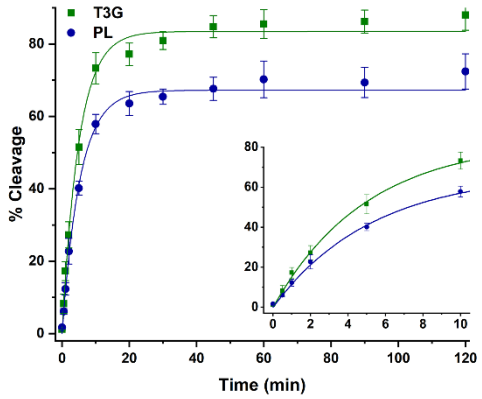

Figure S7, related to Figure 5. Cleavage yields of T3G and PL over the time in the presence of GSH/Cu^{2+}. 0.5 μM T3G (or PL) was incubated with 100 μM GSH/Cu^{2+} at 23 °C in a mixture containing 0.2 M NaCl and 50 mM MES (pH 6.4). The error bars represented the standard deviations from three repeated measurements.

Table S1, related to Figure 3. Sequences of the PL DNAzyme and its single-point mutations.

No.	ID.	Sequences of DNA（5'→3'）
0	PL	GAGATCTTTCTAATACGACTCAGAATGAGTCTGGGCCTCTTTCTTTTAGAAAGAAC
1	A1/2X	GAGATCTTTCTXATACGACTCAGAATGAGTCTGGGCCTCTTTCTTTTAGAAAGAAC
2	T3X	GAGATCTTTCTAAXACGACTCAGAATGAGTCTGGGCCTCTTTCTTTTAGAAAGAAC
3	A4X	GAGATCTTTCTAATXCGACTCAGAATGAGTCTGGGCCTCTTTCTTTTAGAAAGAAC
4	C5X	GAGATCTTTCTAATAXGACTCAGAATGAGTCTGGGCCTCTTTCTTTTAGAAAGAAC
5	G6X	GAGATCTTTCTAATACXACTCAGAATGAGTCTGGGCCTCTTTCTTTTAGAAAGAAC
6	C7X	GAGATCTTTCTAATACGACTCAGAATGAGTXTGGGCCTCTTTCTTTTAGAAAGAAC
7	T8X	GAGATCTTTCTAATACGACTCAGAATGAGTCXGGGCCTCTTTCTTTTAGAAAGAAC
8	G9/10/11X	GAGATCTTTCTAATACGACTCAGAATGAGTCTXGGCCTCTTTCTTTTAGAAAGAAC
9	C12/13X	GAGATCTTTCTAATACGACTCAGAATGAGTCTGGGXCTCTTTCTTTTAGAAAGAAC
10	A14X	GAGATCTTTCTAATACGACTCAGAATGAGTCTGGGCCTCTTTCTTTTAGAAAGAXC
11	C15X	GAGATCTTTCTAATACGACTCAGAATGAGTCTGGGCCTCTTTCTTTTAGAAAGAAX
12	A1G	GAGATCTTTCTGATACGACTCAGAATGAGTCTGGGCCTCTTTCTTTTAGAAAGAAC
13	A1C	GAGATCTTTCTCATACGACTCAGAATGAGTCTGGGCCTCTTTCTTTTAGAAAGAAC
14	A1T	GAGATCTTTCTTATACGACTCAGAATGAGTCTGGGCCTCTTTCTTTTAGAAAGAAC
15	A2G	GAGATCTTTCTAGTACGACTCAGAATGAGTCTGGGCCTCTTTCTTTTAGAAAGAAC
16	A2C	GAGATCTTTCTACTACGACTCAGAATGAGTCTGGGCCTCTTTCTTTTAGAAAGAAC
17	A2T	GAGATCTTTCTATTACGACTCAGAATGAGTCTGGGCCTCTTTCTTTTAGAAAGAAC
18	T3A	GAGATCTTTCTAAAACGACTCAGAATGAGTCTGGGCCTCTTTCTTTTAGAAAGAAC
19	T3G	GAGATCTTTCTAAGACGACTCAGAATGAGTCTGGGCCTCTTTCTTTTAGAAAGAAC
20	T3C	GAGATCTTTCTAACACGACTCAGAATGAGTCTGGGCCTCTTTCTTTTAGAAAGAAC
21	A4G	GAGATCTTTCTAATGCGACTCAGAATGAGTCTGGGCCTCTTTCTTTTAGAAAGAAC
22	A4C	GAGATCTTTCTAATCCGACTCAGAATGAGTCTGGGCCTCTTTCTTTTAGAAAGAAC

23	A4T	GAGATCTTTCTAATTCGACTCAGAATGAGTCTGGGCCTCTTTCTTTTAGAAAGAAC
24	C5A	GAGATCTTTCTAATAAGACTCAGAATGAGTCTGGGCCTCTTTCTTTTAGAAAGAAC
25	C5G	GAGATCTTTCTAATAGGACTCAGAATGAGTCTGGGCCTCTTTCTTTTAGAAAGAAC
26	C5T	GAGATCTTTCTAATATGACTCAGAATGAGTCTGGGCCTCTTTCTTTTAGAAAGAAC
27	G6A	GAGATCTTTCTAATACAACTCAGAATGAGTCTGGGCCTCTTTCTTTTAGAAAGAAC
28	G6C	GAGATCTTTCTAATACCACTCAGAATGAGTCTGGGCCTCTTTCTTTTAGAAAGAAC
29	G6T	GAGATCTTTCTAATACTACTCAGAATGAGTCTGGGCCTCTTTCTTTTAGAAAGAAC
30	C7A	GAGATCTTTCTAATACGACTCAGAATGAGTATGGGCCTCTTTCTTTTAGAAAGAAC
31	C7G	GAGATCTTTCTAATACGACTCAGAATGAGTGTGGGCCTCTTTCTTTTAGAAAGAAC
32	C7T	GAGATCTTTCTAATACGACTCAGAATGAGTTTGGGCCTCTTTCTTTTAGAAAGAAC
33	T8A	GAGATCTTTCTAATACGACTCAGAATGAGTCAGGGCCTCTTTCTTTTAGAAAGAAC
34	T8G	GAGATCTTTCTAATACGACTCAGAATGAGTCGGGGCCTCTTTCTTTTAGAAAGAAC
35	T8C	GAGATCTTTCTAATACGACTCAGAATGAGTCCGGGCCTCTTTCTTTTAGAAAGAAC
36	G9A	GAGATCTTTCTAATACGACTCAGAATGAGTCTAGGCCTCTTTCTTTTAGAAAGAAC
37	G9C	GAGATCTTTCTAATACGACTCAGAATGAGTCTCGGCCTCTTTCTTTTAGAAAGAAC
38	G9T	GAGATCTTTCTAATACGACTCAGAATGAGTCTTGGCCTCTTTCTTTTAGAAAGAAC
39	G10A	GAGATCTTTCTAATACGACTCAGAATGAGTCTGAGCCTCTTTCTTTTAGAAAGAAC
40	G10C	GAGATCTTTCTAATACGACTCAGAATGAGTCTGCGCCTCTTTCTTTTAGAAAGAAC
41	G10T	GAGATCTTTCTAATACGACTCAGAATGAGTCTGTGCCTCTTTCTTTTAGAAAGAAC
42	G11A	GAGATCTTTCTAATACGACTCAGAATGAGTCTGGACCTCTTTCTTTTAGAAAGAAC
43	G11C	GAGATCTTTCTAATACGACTCAGAATGAGTCTGGCCCTCTTTCTTTTAGAAAGAAC
44	G11T	GAGATCTTTCTAATACGACTCAGAATGAGTCTGGTCCTCTTTCTTTTAGAAAGAAC
45	C12A	GAGATCTTTCTAATACGACTCAGAATGAGTCTGGGACTCTTTCTTTTAGAAAGAAC
46	C12G	GAGATCTTTCTAATACGACTCAGAATGAGTCTGGGGCTCTTTCTTTTAGAAAGAAC
47	C12T	GAGATCTTTCTAATACGACTCAGAATGAGTCTGGGTCTCTTTCTTTTAGAAAGAAC
48	C13A	GAGATCTTTCTAATACGACTCAGAATGAGTCTGGGCATCTTTCTTTTAGAAAGAAC
49	C13G	GAGATCTTTCTAATACGACTCAGAATGAGTCTGGGCGTCTTTCTTTTAGAAAGAAC
50	C13T	GAGATCTTTCTAATACGACTCAGAATGAGTCTGGGCTTCTTTCTTTTAGAAAGAAC
51	A14G	GAGATCTTTCTAATACGACTCAGAATGAGTCTGGGCCTCTTTCTTTTAGAAAGAGC
52	A14C	GAGATCTTTCTAATACGACTCAGAATGAGTCTGGGCCTCTTTCTTTTAGAAAGACC
53	A14T	GAGATCTTTCTAATACGACTCAGAATGAGTCTGGGCCTCTTTCTTTTAGAAAGATC
54	C15A	GAGATCTTTCTAATACGACTCAGAATGAGTCTGGGCCTCTTTCTTTTAGAAAGAAA
55	C15G	GAGATCTTTCTAATACGACTCAGAATGAGTCTGGGCCTCTTTCTTTTAGAAAGAAG
56	C15T	GAGATCTTTCTAATACGACTCAGAATGAGTCTGGGCCTCTTTCTTTTAGAAAGAAT

Note: Green characters indicate the nucleotides within catalytic core of PL. Red characters indicate the mutated nucleotides, X indicate the deleted nucleotides. Mutations A1/2X, G9/10/11X, C12/13X indicate the nucleotide deletion occurring at several neighboring positions, resulting in only one PL mutation.

Transparent Methods

Reagents and chemicals

All DNA oligonucleotides (PL and variants) were purchased from Sangon Biotech Co., Ltd. (Shanghai, China) and purified by denaturing PAGE (Table S1). GelRed was purchased from Biotium Inc. Chemical compounds (Figure 2A and 2C) were of analytical reagent grade. Double distilled water was used throughout the experiments.

Self-cleavage assay of PL

In the “Multiple cofactors of PL”section, DNA self-cleavage assay was performed in 100 μL reaction solution containing 0.5 μM PL, 100 μM compound, 100 μM Cu^{2+} (or none), 300 mM NaCl and 50 mM Tris-HCl (pH 7.0) at 23 °C. The reaction system containing VB_2 or FMN needs to be performed in white light.

In the “Mapping the catalytic core of PL” section, DNA self-cleavage assay was performed in 100 μL reaction solution containing 0.5 μM PL mutants, 100 μM Cu^{2+}, 100 μM VC (GSH, PG or HA), 300 mM NaCl and 50 mM Tris-HCl (pH 7.0) at 23 °C.

In the “Characterization of T3G” section, the reaction conditions vary a lot. In Figure 4, DNA self-cleavage assay was performed in 100 μL reaction solution containing 0.5 μM PL (or T3G), 100 μM compound, 100 μM Cu^{2+} (or none), 300 mM NaCl and 50 mM Tris-HCl (pH 7.0) at 23 °C. In Figure 5A, DNA self-cleavage assay was performed in 100 μL reaction solution containing 0.5 μM T3G, 100 μM NADH (or GSH), 100 μM Cu^{2+}, 300 mM NaCl and pH buffer at 23 °C. pH buffer solutions: 200 mM HAc-NaAc (pH 5.0, 5.4, 5.8), 50 mM MES (pH 6.0, 6.4, 6.8) and 50 mM Tris-HCl (pH 7.0, 7.4, 7.8, 8.0, 8.4, 8.8, 9.0). In Figure 5B, DNA self-cleavage assay was performed in 100 μL reaction solution containing 0.5 μM T3G, 100 μM NADH (or GSH), 100 μM Cu^{2+}, 50 mM MES (pH 6.4) and different concentrations of NaCl or KCl (1, 10, 50, 100, 200, 300, 400, 500, 800 and 1000 mM). In Figure 5C, DNA self-cleavage assay was performed in 100 μL reaction solution containing 0.5 μM T3G, 100 μM NADH (or GSH), 100 μM Cu^{2+},1 (or 0.2) M NaCl and 50 mM MES (pH 6.4), at different incubation temperatures (8, 12, 16, 20, 23, 28, 32, 37 and 40 °C). In Figure 5D, NADH/Cu^{2+} concentration dependent experiments were conducted in 100 μL reaction solution containing 0.5 μM T3G, 1 M NaCl,

50 mM MES (pH 6.4), and equal concentration of NADH and Cu^{2+} (1, 5, 10, 50, 100, 500 μM, 1, 5, 10 mM) at 23 °C. GSH/Cu^{2+} concentration dependent experiments were conducted in 100 μL reaction solution containing 0.5 μM T3G, 0.2 M NaCl, 50 mM MES (pH 6.4), and equal concentration of GSH and Cu^{2+} (1, 5, 10, 50, 100, 500 μM, 1, 5, 10 mM) at 23 °C. NADH concentration dependent experiments were conducted in 100 μL reaction solution containing 0.5 μM T3G, 1 M NaCl, 50 mM MES (pH 6.4), and different concentration of NADH (1, 5, 10, 50, 100, 500 μM, 1, 5, 10 mM) at 23 °C. GSH concentration dependent experiments were conducted in 100 μL reaction solution containing 0.5 μM T3G, 0.2 M NaCl, 50 mM MES (pH 6.4) and different concentration of GSH (1, 5, 10, 50, 100, 500 μM, 1, 5, 10 mM) at 23 °C. Cu^{2+}-1M NaCl concentration dependent experiments were conducted in 100 μL reaction solution containing 0.5 μM T3G, 1 M NaCl, 50 mM MES (pH 6.4) and different concentration of Cu^{2+} (1, 5, 10, 50, 100, 500 μM, 1, 5, 10 mM) at 23 °C. Cu^{2+}-0.2 M NaCl concentration dependent experiments were conducted in 100 μL reaction solution containing 0.5 μM T3G, 0.2 M NaCl, 50 mM MES (pH 6.4) and different concentration of Cu^{2+} (1, 5, 10, 50, 100, 500 μM, 1, 5, 10 mM) at 23 °C. In Figure 5E, DNA self-cleavage assay was performed in 100 μL reaction solution containing 0.5 μM T3G, NADH (or GSH), 100 μM Cu^{2+}, 1 (or 0.2) M NaCl, 50 mM MES (pH 6.4), different concentrations of NADH or GSH (1, 5, 10, 50, 100, 500 μM, 1, 5, 10 mM) at 23 °C. In Figure 5F, DNA self-cleavage assay was performed in 100 μL reaction solution containing 0.5 μM T3G, 100 μM NADH (or GSH), 1 (or 0.2) M NaCl, 50 mM MES (pH 6.4) and different concentrations of Cu^{2+} (1, 5, 10, 50, 100, 500 μM, 1, 5, 10 mM) at 23 °C. In Figure 6, DNA self-cleavage assay was performed in 100 μL reaction solution containing 0.5 μM T3G, 100 μM NADH (or GSH), 100 μM metal ions, 1 (or 0.2) M NaCl and 50 mM MES (pH 6.4) at 23 °C.

Analysis of the cleavage products

The reaction mixture was incubated at 23 °C for 1 hr and stopped by adding precipitants (200 μL 100% ethanol, 10 μL 3 M NaOAc (pH 5.2), 1 μL 10 mg/mL glycogen) for precipitation at -20 °C for 20 min. Centrifuge at 14000 rpm for 10 min and air dry the pellets. The dried samples were dissolved in 20 μL loading buffer (4 M Urea, 10 mM EDTA, 25 mM Tris-HCl pH 7.5, 0.125 ‰ xylene cyanol FF, 0.125 ‰ bromophenol blue) and separated by 20 % denaturing polyacrylamide gel electrophoresis (PAGE). Gel was stained with 3× GelRed for 10 min at room temperature. The gels were scanned using Gel Doc XR+ imaging system (Bio-Rad Laboratories Co., Ltd.), and the product bands were

quantified using the Image Lab 6.0 software (Bio-Rad Laboratories Co., Ltd.). The cleavage yield was determined by the equation: % Cleavage=all cleaved fragments/(non-cleaved fragments + all cleaved fragments)×100 %.

Relative drift intensity (RDI) calculation

$RDI=(C_X-C_0)/C_0\times100\%$

$C_0=(C_{N1}+C_{N2}+C_{N3}+C_{N4})/4$, C_0 indicates the average cleavage yield of single nucleotide variants at N position, in the presence of VC/Cu^{2+}.

$C_X=(C_{n1}+C_{n2}+C_{n3}+C_{n4})/4$, C_X indicates the average cleavage yield of single nucleotide variants at N position, at each condition of GSH/Cu^{2+}, PG/Cu^{2+} and HA/Cu^{2+}.

Kinetic analysis

All kinetic values were determined in a similar manner that the incubation time was up to 120 minutes. At specific time points, 100 µL aliquots were removed from the reaction mixture and quenched by mixing with ice-cold stop buffer (200 µL 100% ethanol, 10 µL 3 M NaOAc (pH 5.2), 1 µL 10 mg/mL glycogen). Cleavage products were analyzed by 20 % denaturing polyacrylamide gel electrophoresis. Data were fit to the exponential equation $Y = Y_{max}(1-e^{-kt})$ using non-linear regression in OriginPro 2018 (Wang et al., 2014; Wang et al., 2019). Y was the fraction of reacted self-cleavage DNAzyme, Y_{max} was the maximal yield, k was the observed rate constant (k_{obs}) and t was reaction time. The observed rate constant (k_{obs}) and maximum cleavage yield (Y_{max}) were determined from the regression curve.

Supplemental references

Wang, M., Zhang, H., Zhang, W., Zhao, Y., Yasmeen, A., Zhou, L., Yu, X., and Tang, Z. (2014). *In vitro* selection of DNA-cleaving deoxyribozyme with site-specific thymidine excision activity. Nucleic Acids Res. *42*, 9262−9269.

Wang, Y., Yang, J., Yuan, X., Cao, J., Xu, J., Chaput, J.C., Li, Z., and Yu, H. (2019). A novel small RNA-cleaving deoxyribozyme with a short binding arm. Sci. Rep. *9*, 8224.